

# Nonadiabatic effect in high order harmonic generation revealed by a fully analytical method

Fengjian Sun,<sup>1,2,3,4</sup> Pei Huang,<sup>1,2,\*</sup> Alexandra S. Landsman,<sup>5</sup> Yanpeng Zhang,<sup>3</sup> Liang-Wen Pi,<sup>1,2,†</sup> and Yuxi Fu<sup>1,2,‡</sup>

<sup>1</sup>State Key Laboratory of Ultrafast Optical Science and Technology,

Xi'an Institute of Optics and Precision Mechanics, Chinese Academy of Sciences, Xi'an 710119, Shaanxi, China

<sup>2</sup>Center for Attosecond Science and Technology, Xi'an Institute of Optics and Precision Mechanics,  
Chinese Academy of Sciences, Xi'an 710119, Shaanxi, China

<sup>3</sup>Key Laboratory for Physical Electronics and Devices of the Ministry of Education & Shaanxi  
Key Lab of Information Photonic Technique, Xi'an JiaoTong University, Xi'an 710049, China

<sup>4</sup>University of Chinese Academy of Science, Beijing 100049, China

<sup>5</sup>Department of Physics, the Ohio State University, Columbus, OH 43210, USA

We propose a fully analytical method for describing high-order harmonic generation (HHG). This method is based on the strong-field approximation (SFA) and utilizes the perturbation expansion method. Specifically, we expand the laser-induced dipole moment to third-order analytical expansion (TAE) and fifth-order expansion (FAE) with respect to the Keldysh parameter  $\gamma$ . The TAE method is suitable for  $\gamma \leq 0.27$ , while the FAE method can be applied for  $\gamma \leq 0.65$ . We demonstrate that higher-order perturbation terms capture the nonadiabatic effect, while the zero-order term represents the adiabatic effect. Furthermore, we reveal that the nonadiabatic effect influences HHG intensity by impacting electron dynamics.

## I. INTRODUCTION

When a laser interacts with gases, complex high order nonlinear effects occur, leading to the HHG. Since the 1980s, extreme ultraviolet (EUV) HHG have been observed when rare gases are driven by near-infrared intense laser fields [1–3]. HHG has attracted a lot of attention in the field of optics. In recent decades, HHG from solids [4–8] and liquids [9–12] have also been extensively investigated. As an important method for producing coherent EUV light, HHG is predicted to have the ability to generate attosecond pulses [13], which have been observed in experiments [14, 15]. Additionally, HHG can be used to probe electron dynamics and molecular structure [16–18]. Furthermore, high photon energy HHG also have the potential to serve as a light source for extreme ultraviolet lithography machines [19].

To understand the complex mechanisms of HHG, the SFA method was proposed [20] and has since been widely adopted [21–23]. The SFA method typically performs well under the assumption of considering only the ground state in bound states, neglecting the depletion of the ground state, and ignoring the Coulomb effect. It is especially effective in the case of low-frequency driving lasers with a small Keldysh parameter [24],  $\gamma \equiv \omega \sqrt{2I_p}/E_0$ , where  $\omega$ ,  $E_0$ , and  $I_p$  represent the laser frequency (also photon energy in atomic units), peak electric field strength, and binding energy of the target atom, respectively. To gain clearer insights into the characteristics of HHG, numerical solutions of saddle point equations [20, 25] and the quantum electron trajectory theory [26–28] are employed in this method.

Commonly, ionization is the first step of HHG. It determines the initial conditions of electron dynamics out of the barrier, and influences HHG yields significantly. The ioniza-

tion process is usually characterized by the Keldysh parameter, also known as the adiabatic parameter [29], which can be expressed as  $\gamma \equiv \omega/\omega_t$ , where  $\omega_t \equiv E_0/\sqrt{2I_p}$  [24]. When  $\gamma \ll 1$ , ionization can be treated as an adiabatic case, and this process can be described in adiabatic approximation. In the range of intermediate  $\gamma \sim 1$ , which is typical for many current intense field experiments, this process will be greatly influenced by the nonadiabatic effect. In 1966, the PPT theory was proposed to evaluate the ionization yield [29], taking the nonadiabatic effect into account. By using the adiabatic limit condition  $\gamma \ll 1$ , the probability of ionization results from averaging the probabilities of ionization in fields over a period of the external field, which is suitable for the adiabatic region. In 1986, these theories were further summarized and the ADK theory was proposed, which works well especially in the adiabatic region and has been widely adopted [30].

Following these pioneering theoretical works, the adiabatic approximation and nonadiabatic effects in the ionization process have garnered a lot of attention. Many studies were subsequently carried out to investigate the ionization process in comparison to experimental results. In reference [31], a calculation based on the adiabatic limit condition was presented, showing good agreement with experimental results for Kr in a linearly polarized laser field [32]. Additionally, it was found that the tunneling exit momentum is zero in the adiabatic limit but nonzero in the nonadiabatic region. This characteristic has been widely adopted in theoretical and experimental analyses [33–37], making it a useful tool in distinguishing between adiabatic and nonadiabatic methods. Under the adiabatic approximation, the barrier is quasi-static, and the electron energy beneath the barrier always equals the binding energy  $I_p$ . However, in the case of nonadiabatic processes, the electron undergoes changes while tunneling, resulting in the electron energy at the tunneling exit not being equal to  $I_p$ , which is a key characteristic of nonadiabatic theory.

In recent years, various experiments have been conducted to study the nonadiabatic effect in the ionization process [33, 35, 38–40]. Additionally, some analytical work has also been carried out to explore this phenomenon [41–43]. But

\* huangpei@opt.ac.cn

† lwpi@opt.ac.cn

‡ fuyuxi@opt.ac.cn

in reference [39], a contradictory conclusion was presented, suggesting that for a wide range of intensities, nonadiabatic theories proposed do not align with experimental data trends, while adiabatic assumptions are supported. So further investigation into the ionization process is still necessary. Meanwhile, recent studies have focused on HHG to analyze the yield in both adiabatic and nonadiabatic regions [44, 45], with some research concentrating on electron dynamics [46–48]. However, there is still a lack of comprehensive analytical work on the nonadiabatic effect in the HHG process, making it challenging to differentiate between the contributions of adiabatic and nonadiabatic effects on HHG spectra.

In this paper, a fully analytical method based on SFA and the saddle point method to describe HHG is proposed. This method allows for the calculation of HHG without the need to numerically solve the saddle point equations (Sec. II). The accuracy of the analytical method is confirmed by comparing it to the results obtained from numerically solving the saddle point equation of SFA (Sec. III). Our method separates the nonadiabatic effect and adiabatic effect naturally, with the zero-order expansion term representing an adiabatic description, and higher-order expansion terms representing a nonadiabatic description. The analytical method is able to provide nonadiabatic initial conditions for electron at the tunneling exit, which influences the following dynamics of electron and HHG yield (Sec. IV). Lastly, a conclusion is drawn (Sec. V).

## II. ANALYTICAL DESCRIPTION

According to SFA, when an atom is driven by the laser field  $\mathbf{E}(t)$ , the component of the time-dependent dipole moment along an arbitrary direction  $\mathbf{n}$  can be expressed as [20].

$$D_{\mathbf{n}}(t) = i \int_0^t dt' \int d^3\mathbf{p} \, \mathbf{n} \cdot \mathbf{d}_r^*(\mathbf{p} - \mathbf{A}(t)) \times \mathbf{E}(t') \cdot \mathbf{d}_i^*(\mathbf{p} - \mathbf{A}(t')) \exp[-iS(\mathbf{p}, t, t')] + c.c. \quad (1)$$

Here,  $\tau \equiv t - t'$  representing the excursion time of the ionized electron, with  $t'$  and  $t$  being the ionization and return time respectively. The vector potential of the field is denoted as  $\mathbf{A}(t)$ , satisfying the relation  $\mathbf{A}(t) \equiv -\int_{-\infty}^t \mathbf{E}(t'') dt''$ . The canonical momentum is denoted as  $\mathbf{p}$ . In Equation (1),  $\mathbf{d}_i(\mathbf{p} - \mathbf{A}(t'))$  represents the dipole transition matrix element between the ground state and the continuum state  $|\mathbf{p} - \mathbf{A}(t')\rangle$ . Similarly,  $\mathbf{d}_r^*(\mathbf{p} - \mathbf{A}(t))$  represents that from the continuum state  $|\mathbf{p} - \mathbf{A}(t)\rangle$  to the ground state.  $S$  is the quasiclassical action [20], describing the free electron motion driven by the laser field and has the expression:

$$S = \int_{t'}^t \left( \frac{[\mathbf{p} - \mathbf{A}(t'')]^2}{2} + I_p \right) dt''. \quad (2)$$

The primary contribution to the integral in Eq. (1) arises from the saddle points of the action, which can be derived from the quasiclassical action. With respect to  $\mathbf{p}$ , one can de-

rive a saddle point equation:

$$\nabla_{\mathbf{p}} S = \int_{t'}^t [\mathbf{p} - \mathbf{A}(t'')] dt'' = 0. \quad (3)$$

Then one can obtain the saddle point canonical momentum

$$\mathbf{p}_s = \frac{1}{t - t'} \int_{t'}^t \mathbf{A}(t'') dt''. \quad (4)$$

Assuming the laser is linearly polarized in the  $x$ -axis, then the saddle point canonical momentum is apparently along the  $x$ -axis as well. By combining the saddle point method with Eq. (1), it can be simplified to a one-dimensional form:

$$D_x(t) = -i \int_{-\infty}^t dt' [\xi(\tau) d_r^*(p_s - A(t)) \times E(t') \cdot d_i(p_s - A(t')) \times e^{-iS(p_s, t, t')}] + c.c.. \quad (5)$$

The factor  $\xi(\tau) = [\pi/(\epsilon' + i\tau/2)]^{\frac{3}{2}}$  arises from the Gaussian integration around the saddle points, where  $\epsilon'$  is an infinitesimal quantity used to prevent numerical singularities.  $\xi(\tau)$  accurately describes the spread of the electronic wave packet. Therefore, the Fourier transform of  $D_x(t)$  has the form specified in reference [49]

$$D_x(\Omega) = -i \int dt \int_{-\infty}^t dt' [\xi(\tau) d_r^*(p_s - A(t)) \times E(t') \cdot d_i(p_s - A(t')) \times e^{-i\Theta(p_s, t, t')}] \quad (6)$$

In the equation above, the exponential term  $\Theta(p_s, t, t')$  has the following form:

$$\Theta(p_s, t, t') = S(p_s, t, t') - \Omega t / \omega. \quad (7)$$

Here,  $\Omega$  represents the photon energy of the HHG, which can be expressed as the sum of the kinetic energy of returned electron and the binding energy of the target atom. Similarly, using Eq. (3), one can derive the other two saddle point equations from  $\Theta$  with respect to  $t'$  and  $t$ :

$$\frac{[p_s - A(t')]^2}{2} + I_p = 0, \quad (8)$$

$$\frac{[p_s - A(t)]^2}{2} - (\Omega - I_p) = 0. \quad (9)$$

By solving the two equations above, one can obtain a pair of saddle points  $(t_r, t_i)$  for a given photon energy  $\Omega$  of an electron quantum trajectory. Here,  $t_r$  represents the saddle point return time and  $t_i$  represents the saddle point ionization time. According to quantum trajectory theory, the induced dipole of a certain trajectory can be denoted as  $D_{xj}(\Omega)$ . The laser-induced time-dependent dipole moment along the laser

polarization [49] for the quantum trajectory can be expressed as

$$D_{xj}(\Omega) = \xi(\tau) \frac{2\pi}{\sqrt{\det(S'')}} d_r^*(p_s - A(t_r)) \times E(t_i) d_i(p_s - A(t_i)) e^{-i\Theta(p_s, t_r, t_i)}. \quad (10)$$

In this context, the subscript “j” represents different trajectories, such as “S1” refers to the short trajectory in the first return, “L1” refers to the long trajectory in the first return, “S2” refers to the short trajectory in the second return and so forth. Therefore, the intensity of the HHG spectra can be expressed as

$$P(\Omega) \propto \left| \sum_j D_{xj}(\Omega) \right|^2. \quad (11)$$

According to SFA, the three saddle point equations provide three key quantities:  $p_s$ ,  $t_r$  and  $t_i$  and these three quantities dominate the HHG process. Based on the theory outlined above, a detailed form of the laser field can be introduced to obtain the fully analytical results.

The linearly polarized laser can be assumed to be a monochromatic field, where  $E(t) = E_0 \cos(t)$ . Here, the independent variable  $t$  represents the phase and will be used in the following text. Similarly, time-related variables such as electron return time, ionization, and excursion are also presented in this form. By utilizing Eq. (4) and the expression  $E(t) = E_0 \cos(t)$ , one can easily derive the canonical momentum as

$$p_s = A_0 \cdot \frac{[\cos(t_r) - \cos(t_r - \tau)]}{\tau}. \quad (12)$$

Here,  $A_0$  satisfies the relation  $A_0 = 2\sqrt{U_p}$ . Similarly, the adiabatic parameter  $\gamma$  mentioned in the first section can also be written as a function of  $U_p$ , such that  $\gamma = \sqrt{I_p/2U_p}$ . The relationship between  $U_p$  and  $\gamma$  suggests that  $U_p$  is a suitable scaling quantity of energy when expanding quantities with respect to  $\gamma$ , therefore  $A_0$  is a suitable scaling quantity of momentum. By scaling with  $U_p$  and utilizing Eq. (12), Eq. (8) can be simplified to a concise and equivalent form that expresses the relationship between  $t_r$  and  $\tau$  in the following expression (the detailed derivation process can be found in appendix A)

$$\sin\left(t_r - \frac{\tau}{2}\right) a - \cos\left(t_r - \frac{\tau}{2}\right) s = i\gamma. \quad (13)$$

Here  $a$  and  $s$  are defined as

$$a \equiv a(\tau) = \cos(\tau/2) - \frac{2\sin(\tau/2)}{\tau}, \quad (14)$$

$$s \equiv s(\tau) = \sin(\tau/2).$$

Similarly, scaling with  $U_p$  and utilizing Eqs. (12, 13), equation (9) can be simplified. Then the kinetic energy of the returned electron can be expressed as a function of  $\tau$  (the de-

tailed derivation process can be found in appendix B).

$$E_{re} = \frac{(p_s - A(t_r))^2}{2} = 2U_p \left[ a \frac{ia\gamma + (s\sqrt{a^2 + s^2 + \gamma^2})}{a^2 + s^2} - is\gamma + \left( a\sqrt{a^2 + s^2 + \gamma^2} \right) + s \frac{-is\gamma + (a\sqrt{a^2 + s^2 + \gamma^2})}{a^2 + s^2} \right]^2. \quad (15)$$

Here, the kinetic energy of the returned electron satisfies the relationship  $E_{re} = \Omega - I_p$ . According to Eq. (14) and Eq. (15),  $E_{re}$  is a function of the excursion  $\tau$  only. Therefore, the  $\tau$  can be expanded to a third-order expansion as:

$$\tau^{(3)} = \tau_0 + \tau_1\gamma + \tau_2\gamma^2 + \tau_3\gamma^3, \quad (16)$$

where  $\tau = \tau^{(3)} + O(\gamma^4)$ . By replacing  $\tau$  with  $\tau^{(3)}$  and considering the third-order expansion with respect to  $\gamma$ , the kinetic energy of electron at the return time can be expanded to a third-order form:

$$E_{re}^{(3)} = U_p \cdot (E_{re0} + \gamma E_{re1} + \gamma^2 E_{re2} + \gamma^3 E_{re3}). \quad (17)$$

In experiments, as an observable quantity,  $E_{re}$  must be a real value, meaning that  $\text{Im}[E_{re}] = 0$ . By applying this condition to Eq. (17), the coefficient of the second-order term is derived to be  $\tau_2 = 0$ , and  $\tau_1$  and  $\tau_3$  in Eq. (16) are shown to be imaginary. To make the results clearer, we will redefine  $\tau_1$  and  $\tau_3$  as the real coefficients of the imaginary first and third-order terms, thereby collating the third-order expansion of the excursion time  $\tau$

$$\tau^{(3)} = \tau_0 + i\tau_1\gamma + i\tau_3\gamma^3, \quad (18)$$

where the coefficients of higher-order expansion terms, which are functions of  $\tau_0$  take the following forms:

$$\tau_1 = -\frac{\tau_0 \sqrt{a_0^2 + s_0^2}}{2a_0s_0 + \tau_0(a_0^2 + s_0^2)},$$

$$\tau_3 = \frac{\tau_0 \sqrt{a_0^2 + s_0^2}}{6(a_0^2 - s_0^2)(a_0^2\tau_0 + 2a_0s_0 + s_0^2\tau_0)^4} \times [a_0^6\tau_0^3 + 2a_0^5s_0\tau_0^2 + a_0^4s_0^2\tau_0(\tau_0^2 - 6) - 12a_0^3s_0^3 - a_0^2s_0^4\tau_0(\tau_0^2 - 20) - 2a_0s_0^5(\tau_0^2 - 6) - s_0^6\tau_0(\tau_0^2 - 2)]. \quad (19)$$

Here,  $a_0 \equiv a(\tau_0)$  and  $s_0 \equiv s(\tau_0)$ . By inserting this expression of  $\tau_3$  into Eq. (15) again, and expanding it to third order with respect to  $\gamma$ , one can obtain the expression of  $E_{re}^{(3)}$  as

$$E_{re}^{(3)} = U_p \cdot (E_{re0} + E_{re2}\gamma^2). \quad (20)$$

The coefficients of zero and second order expansions are [50]

$$E_{re0} = \frac{8a_0^2s_0^2}{a_0^2 + s_0^2},$$

$$E_{re2} = -\frac{16a_0^2s_0^3(s_0 + a_0\tau_0)}{(a_0^2 + s_0^2)(2a_0s_0 + a_0^2\tau_0 + s_0^2\tau_0)^2}. \quad (21)$$

According to Eq. (13), the expression of return time  $t_r$  can also be written as a function of  $\tau$  (the detailed derivation is shown in appendix B). Then,  $t_r$  can be expanded to third order directly with respect to  $\gamma$  as

$$t_r^{(3)} = t_{r0} + t_{r2}\gamma^2 + it_{r3}\gamma^3. \quad (22)$$

where the coefficients of the expansions are functions of  $\tau_0$  and have the form of

$$\begin{aligned} t_{r0} &= \tau_0/2 + \arctan(a_0, s_0), \\ t_{r2} &= \frac{\tau_0 \cos \tau_0 - \sin \tau_0}{a_0^2 + s_0^2}, \\ t_{r3} &= \frac{2 \sin(\tau_0/2)^2}{3(\tau_0 - \sin \tau_0)^3} \\ &\quad \times \frac{(2 + \tau_0^2 - 2 \cos \tau_0 - 2\tau_0 \sin \tau_0)^{3/2}}{[2 + (\tau_0^2 - 2) \cos \tau_0 - 2\tau_0 \sin \tau_0]}. \end{aligned} \quad (23)$$

Based on Equations (12), (18), and (22), the canonical momentum  $p_s$  can also be expanded to the third order as

$$p_s^{(3)} = A_0 \cdot (p_{s0} + p_{s2}\gamma^2 + ip_{s3}\gamma^3), \quad (24)$$

where the coefficients of the expansions have the forms of

$$\begin{aligned} p_{s0} &= -\sin(t_{r0} - \tau_0), \\ p_{s2} &= -\frac{\tau_1^2 \cos(t_{r0} - \tau_0)}{2\tau_0} \\ &\quad - \frac{t_{r2} [\sin(t_{r0}) - \sin(t_{r0} - \tau_0)]}{\tau_0}, \\ p_{s3} &= -\frac{1}{6(\tau_0)^2} [(6\tau_0\tau_1t_{r2} - 3\tau_1^3) \cos(t_{r0} - \tau_0) \\ &\quad + 6(\tau_0t_{r3} - \tau_1t_{r2}) \sin(t_{r0}) \\ &\quad + (-6\tau_0t_{r3} + 3\tau_1t_{r2}) \sin(t_{r0} - \tau_0)]. \end{aligned} \quad (25)$$

Based on the expansions mentioned earlier, the saddle point excursion time  $\tau$  and return time  $t_r$  have been expanded to their third-order forms:  $\tau^{(3)}$  and  $t_r^{(3)}$ . By using the relationship  $t_i^{(3)} = t_r^{(3)} - \tau^{(3)}$ , the ionization time can be determined. Therefore, the third-order ionization time is expressed as

$$t_i^{(3)} = t_{i0} + it_{i1}\gamma + t_{i2}\gamma^2 + it_{i3}\gamma^3. \quad (26)$$

In our previous work [50], the second-order analytical electron kinetic energy  $E_{re}$  was obtained, and the influence of the nonadiabatic effect on the cutoff energy of HHG was studied. In this section, with respect to  $\gamma$ , the third-order expansion of the three saddle point quantities  $t_r^{(3)}$ ,  $t_i^{(3)}$  and  $p_s^{(3)}$  has been performed as functions of  $\tau_0$ . In the following sections, the HHG spectra will be further examined based on the derivations of  $t_r^{(3)}$ ,  $t_i^{(3)}$  and  $p_s^{(3)}$ . The applicability of the analytical method will then be discussed in detail, and the nonadiabatic effect on HHG spectra will be demonstrated.

### III. APPLICABILITY OF THE ANALYTICAL METHOD

In the spirit of SFA, the exponential factor  $e^{-i\Theta}$  dominates the dipole moment Eq. (10). To demonstrate the applicability

of this analytical method, we will first discuss the exponential factor  $\Theta$ . This factor is critically important for the HHG yield as it is directly related to the ionization ratio [51]. The variable  $\Theta$  can be scaled by  $U_p/\omega$ , allowing us to define a new variable  $\theta$  that satisfies the relation:

$$\Theta(p_s, t_r, t_i) = \frac{U_p}{\omega} \theta. \quad (27)$$

Then one can expand  $\theta$  to either third-order or fifth-order as a function of  $\tau_0$  that

$$\begin{aligned} \theta^{(3)} &= \theta_0(\tau_0) + \theta_2(\tau_0)\gamma^2 + i\theta_3(\tau_0)\gamma^3, \\ \theta^{(5)} &= \theta^{(3)} + \theta_4(\tau_0)\gamma^4 + i\theta_5(\tau_0)\gamma^5. \end{aligned} \quad (28)$$

Here,  $\theta^{(3)}$  is the third-order analytical expansion (TAE) of  $\theta$  and  $\theta^{(5)}$  is the fifth-order analytical expansion (FAE) of  $\theta$ . Based on our derivation, the even-order expansion terms are real-valued, but the odd-order terms are imaginary-valued.

Then the HHG contribution of a certain quantum trajectory can be expressed as the following:

$$\begin{aligned} |D_{xj}(\Omega)|^2 &\propto e^{2\text{Im}\{\Theta\}} \\ &\propto \exp(\theta_3 \frac{I_p}{\omega} \gamma) \exp(\theta_5 \frac{I_p}{\omega} \gamma^3) \\ &\propto \exp(\sqrt{2}\theta_3 \frac{I_p^{1.5}}{E_0}) \exp(2\sqrt{2}\theta_5 \frac{I_p^{2.5}\omega^2}{E_0^3}). \end{aligned} \quad (29)$$

The imaginary parts of  $\theta$  contribute directly to HHG amplitudes. Here the third-order scaling law and the fifth-order scaling law are derived. Here  $E_0$  and laser intensity  $I_0$  satisfy the relationship of  $E_0^2 \propto I_0$ , hence third-order scaling law is only determined by the binding energy and laser intensity, while the fifth-order scaling law is associated with the wavelength in addition. Theoretically, one needs to at least the TAE to obtain the amplitude of spectra once  $\theta$  has been expanded to the third order. However, obtaining fourth- and fifth-order corrections is necessary further to improve accuracy.

In Fig. 1(a), the third-order expansion of the returned electron kinetic energy,  $E_{re}^{(3)}$ , is plotted as a function of  $\tau_0$ . The horizontal dashed line represents the zero return energy. The intersection of the zero energy line and  $E_{re}^{(3)}$  occurs at  $\tau_0 \approx 0.2$ , indicated by the arrow. It is observed that  $E_{re}^{(3)}$  is positive for almost every trajectory except for the S1 trajectory. In the case of the S1 trajectory,  $E_{re}^{(3)}$  can be low to negative for  $\tau_0 < 0.2$ , indicating that the electron is extremely difficult to return to the core according to quantum trajectory theory. According to the SFA,  $E_{re}^{(3)}$  being smaller than zero corresponds to below-threshold harmonics, and the accuracy of the approximation decreases. Therefore, our analytical method is not suitable for describing the mechanism in this region, and it will not be further discussed in this paper. The figure is divided into different parts by vertical dashed lines to distinguish between different electron quantum trajectories based on the  $E_{re}^{(3)}$  curves.

In Fig. 1(b),  $\theta_3$ , represented by the black solid line, is always negative for all trajectories and changes with  $\tau_0$ . For the

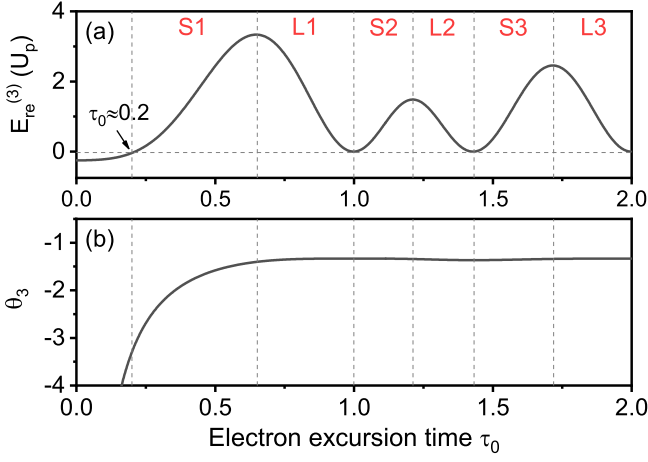


FIG. 1. (a) The returned electron kinetic energy  $E_{re}^{(3)}$  for  $\gamma = 0.5$  and (b) exponential factor coefficients  $\theta_3$  are functions of the electron excursion time  $\tau_0$ .

S1 trajectory,  $\theta_3$  increases rapidly with increasing  $\tau_0$ , potentially leading to a significant change in HHG yields. However, for multiple returns and the L1 trajectory,  $\theta_3$  only oscillates slightly, resulting in stable HHG yields.

In Eq. (29), the negative  $\theta_3$  lay the basis for HHG yields  $\exp(\sqrt{2}\theta_3 \frac{I_p^{1.5}}{E_0})$  and the specific expression of it and its physical meaning will be discussed later in Sec. IV. Our derivation shows that  $\theta_5$  is always positive, so the fifth-order exponential term is always greater than 1, then  $\exp(2\sqrt{2}\theta_5 \frac{I_p^{2.5}\omega^2}{E_0^3})$  which is determined by the  $I_p$ ,  $E_0$  and laser frequency  $\omega$  can be considered as a reinforced correction to the HHG yields and provide a more accurate result.

Figure. 2(a) illustrates the fifth-order correction as a function of  $\tau_0$  and laser intensity  $I_0$ . It is evident that as the  $I_0$  decreases, the fifth-order correction factor increases, indicating that the fifth-order correction to HHG yield becomes more significant. For a 1600 nm laser wavelength, when  $I_0$  is below  $2 \times 10^{14}$  W/cm<sup>2</sup>, the fifth-order correction can boost the HHG yield by over 200%.

In Fig. 2(b), the fifth-order correction is plotted against  $\tau_0$  and laser wavelength. Similar to the previous case, a decrease in wavelength results in a larger fifth-order correction. For a laser intensity of  $I_0 = 1 \times 10^{14}$  W/cm<sup>2</sup>, when the  $\lambda$  is under 2400 nm, the fifth-order correction increase the HHG yield more than 200%. The boundary between S1 and L1 trajectories is indicated by a vertical dashed line in Fig. 2. Generally, the fifth-order correction remains stable for L1 and other multiple return trajectories. However, for the S1 trajectory (region where  $\tau_0 < 0.65$ ), the fifth-order correction increases significantly with decreasing  $\tau_0$ , which make it necessary to include the fifth-order correction when investigating the S1 trajectory.

In order to qualitatively determine the applicability of TAE and FAE in simulating the HHG spectra, we introduce the con-

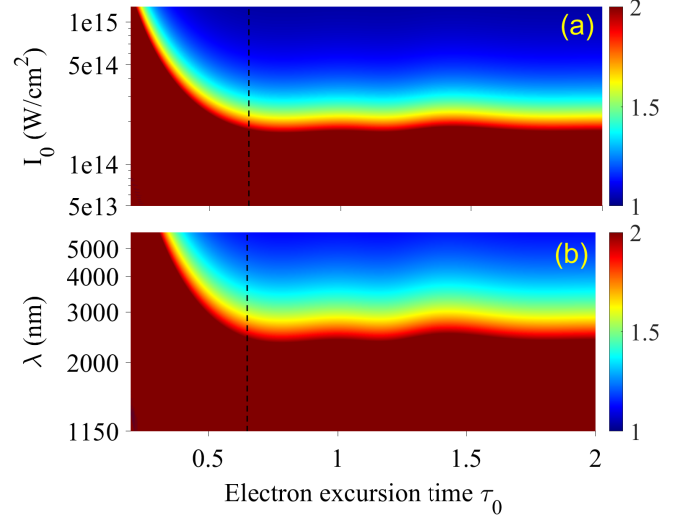


FIG. 2. (a) The fifth-order term is given by  $\exp(2\sqrt{2}\theta_5 \frac{I_p^{2.5}\omega^2}{E_0^3})$  as a function of  $\tau_0$  and  $I_0$ , with  $\lambda = 1600$  nm. (b) The fifth-order term is  $\exp(2\sqrt{2}\theta_5 \frac{I_p^{2.5}\omega^2}{E_0^3})$  as a function of  $\tau_0$  and laser wavelength, with  $I_0 = 1 \times 10^{14}$  W/cm<sup>2</sup>. The target atom is helium. The black dashed line denotes the boundary between the S1 and L1 trajectories.

cept of error rate expressed as:

$$\delta = \frac{|P_j^{(TAE/FAE)}(\Omega_c) - P_j^{(NSFA)}(\Omega_c)|}{P_j^{(NSFA)}(\Omega_c)}. \quad (30)$$

In the equation above, the error rate  $\delta$  of HHG intensity is a relative error. It is defined as the ratio of the difference between NSFA and TAE/FAE results over NSFA results. For the region where the energy is greater than the HHG cutoff energy, the calculation of NSFA for the S1 trajectory will diverge unphysically [51], so the photon energy  $\Omega_c$  chosen here is slightly lower than the cutoff energy to avoid numerical divergence.

As illustrated in Fig. 3, the error rates of the TAE and FAE methods are plotted against the adiabatic parameter  $\gamma$ . The error rates  $\delta$  of the TAE method for the S1 and L1 trajectories are depicted by the black solid and blue short-dashed lines, respectively, while the error rates of the FAE method for the S1 and L1 trajectories are shown by the red dashed and green dash-dotted lines, respectively. It is set that when  $\delta$  is less than 0.1, the analytical calculation of HHG spectra is acceptable, corresponding to the magenta area in Fig. 3. For the TAE method, it is applicable when  $\gamma < 0.27$ , while for the FAE method, it is applicable when  $\gamma < 0.65$ .

As shown in Eq. (11), the HHG yield is a coherent sum of contributions from different quantum trajectories, and the interference between them must be included. The accuracy of the analytical method for describing interference effects in HHG is further confirmed in Fig. 4.

The HHG driven by the near-infrared driving laser with  $\lambda = 1030$  nm and  $\gamma = 0.5$ , obtained from different methods including interference between S1 and L1 trajectories, are

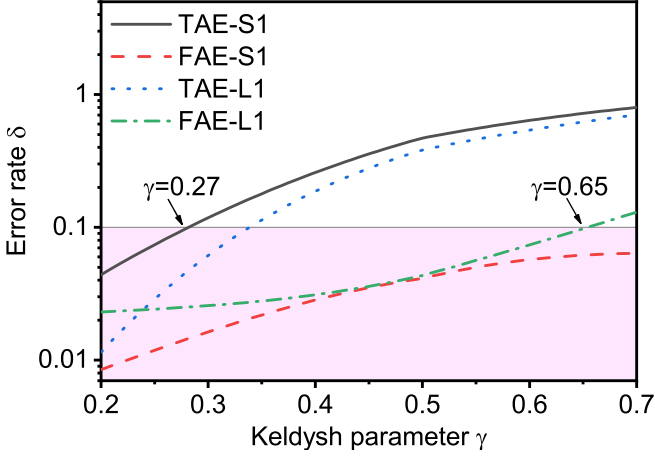


FIG. 3. Error rates of TAE and FAE methods for the first return short and long trajectories vary as a function of the adiabatic parameter  $\gamma$ . The laser wavelength is  $\lambda = 1600 \text{ nm}$ , and the intensity ranges from  $1.05 \times 10^{14} \text{ W/cm}^2$  to  $1.28 \times 10^{15} \text{ W/cm}^2$ , corresponding to the range of  $0.7 \geq \gamma \geq 0.2$ .

compared in Fig. 4 (a). When comparing the black solid line and red dotted line, the harmonic yields of the oscillating peak of NSFA are about 1.4 times higher than those from TAE. However, the comparison with NSFA results shows that the FAE method performs better, resulting in the blue dashed line closely resembling that of NSFA. For a mid-infrared driving laser, it can lead to HHG with higher photon energy extending to the X-ray region, which have a wide range of applications [52, 53].

In Fig. 4(b), comparison between different methods is also shown for mid-infrared laser with  $\lambda = 2500 \text{ nm}$  and  $\gamma = 0.27$ , there are small differences compared to the results of  $\gamma = 0.5$ . In the near cutoff energy regions, the results of TAE and FAE are both in agreement with those of NSFA. The yield calculated by TAE is approximately 10% lower than that of NSFA, which is acceptable for the common HHG calculation. And the FAE result is only 0.4% higher than that of NSFA. Therefore, both methods can accurately describe HHG driven by mid-infrared laser even including the complex interference between different trajectories.

In fact, the difference between FAE and TAE can be attributed to the nonadiabatic effect in the HHG process, which will be discussed further in the next section.

#### IV. NONADIABATIC EFFECT IN HHG PROCESS

In the HHG process, the nonadiabatic effect will first impact the ionization yield, then influences the following electron propagation and return processes. Finally, the nonadiabatic effect will be retained in the HHG yield.

In the TAE method, the third-order term  $\theta^{(3)}$  in Eq. (28)

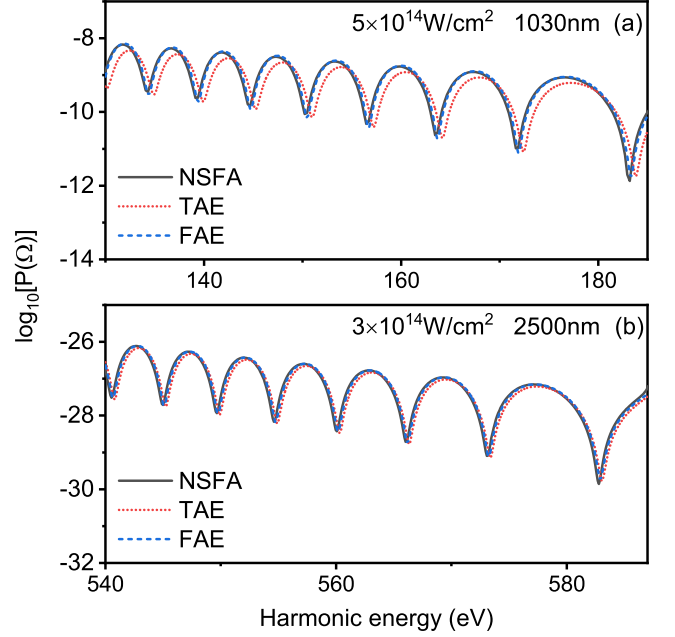


FIG. 4. The HHG spectra of a helium atom were simulated using the NSFA method (black solid lines), TAE method (red dotted lines), and FAE method (blue dashed lines). The HHG in the upper frame were driven by a laser with intensity of  $I = 5 \times 10^{14} \text{ W/cm}^2$  and wavelength of  $\lambda = 1030 \text{ nm}$ , while those in the lower frame were driven by a laser with intensity of  $I = 3 \times 10^{14} \text{ W/cm}^2$  and  $\lambda = 2500 \text{ nm}$ .

and HHG yield can be expressed as

$$\theta_3 = -\frac{4}{3 \cos t_{i0}}, \quad (31)$$

$$\begin{aligned} |D_{xj}(\Omega)|^2 &\propto \exp(\theta_3 \frac{I_p}{\omega} \gamma) \\ &\propto \exp(-\frac{2(2I_p)^{1.5}}{3E_0 \cos t_{i0}}). \end{aligned} \quad (32)$$

Here, third-order term  $\theta_3$  is solely determined by  $t_{i0}$ , which is the zero-order coefficient of ionization time  $t_i$  as in Eq. (26). It suggests that in the TAE method, the HHG yield is determined by the ionization process only, which agrees with ADK theory in adiabatic approximation.

On the other hand, the FAE method includes higher-order term of  $\gamma^3$  in the HHG yield is as follows:

$$|D_{xj}(\Omega)|^2 \propto \exp(\theta_5 \frac{I_p}{\omega} \gamma^3) = \exp(2\sqrt{2}\theta_5 \frac{I_p^{2.5}\omega^2}{E_0^3}). \quad (33)$$

Here an extra dependence on laser frequency  $\omega^2$  is introduced, and this result can then be considered as a nonadiabatic one. The fifth-order coefficient  $\theta_5$  in Eq. (33) is cumbersome and relies on both the ionization time  $t_i$  and the return time  $t_r$  (see Appendix C). When considering the fifth-order expansion, the HHG yield is not only determined by the ionization process,

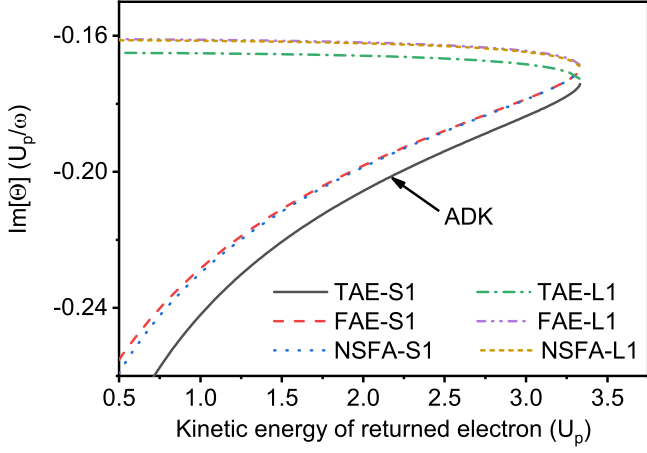


FIG. 5. The exponential factor  $\text{Im}[\Theta]$  as a function of electron return kinetic energy  $E_{re}$  was obtained using different methods when  $\gamma = 0.5$ . The results for the S1 and L1 trajectories obtained by the NSFA method are shown in black solid and red long-dashed lines, while the results from the TAE method are represented by blue dotted and purple dash-dotted lines for the S1 and L1 trajectories, respectively. The results obtained by the FAE method are shown in green dash-dot-dotted and brown short dashed lines for the S1 and L1 trajectories, respectively.

but also the propagation and return processes, leading to a more accurate result.

As shown in Fig. 5, a comparison of HHG amplitudes obtained with different methods is presented. The NSFA is used as a reference, indicated by the black solid and red long-dashed lines, while the results of TAE-S1 and TAE-L1 are represented by the blue dotted and purple dash-dotted lines, respectively. When comparing the NSFA and TAE results, a significant difference is observed at low electron return energy regions for S1 trajectory. This is likely due to the later tunneling exit time in half an optical cycle, resulting in lower instantaneous electric fields at the tunneling exit moment  $t_{ex} = \text{Re}[t_i] \approx t_{i0}$  [54, 55]. Consequently, there is a larger effective adiabatic parameter  $\gamma(t_{ex}) = \omega\sqrt{2I_p}/E(t_{ex})$  [51], indicating a greater nonadiabatic effect. However, as the kinetic energy of returned electron increases, the difference between TAE and NSFA results gets smaller. On the other hand, TAE-L1 consistently performs better in describing HHG amplitude. Compared to NSFA-L1, the results appear closer to each other, likely due to a smaller effective adiabatic parameter  $\gamma(t_{ex}) = \omega\sqrt{2I_p}/E(t_{ex})$ , indicating a reduced nonadiabatic effect. The TAE curves can also be plotted using Eq. (107) in Ref. [49], where the exponential factor is equal to  $-(2I_p)^{3/2}/(3E(t_{ex}))$ , in an ADK-like form when assuming the laser field is static.

Both the FAE-S1 and FAE-L1 curves agree better with NSFA results compared to TAE results in all energy regions. The inclusion of high-order terms in the calculations significantly improves the accuracy of HHG amplitude, especially in low-energy region with larger nonadiabatic effects. It is evident that FAE yields are consistently larger than TAE yields,

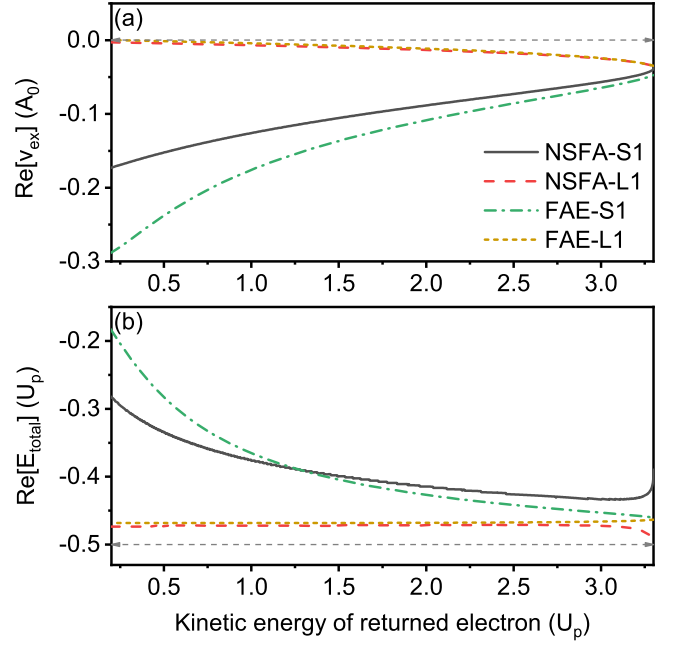


FIG. 6. The real part of the electron velocity at the tunneling exit,  $\text{Re}[v_{ex}]$  (a), and the total energy of the electron at the tunneling exit,  $\text{Re}[E_{total}]$  (b), are shown as functions of the electron return kinetic energy,  $E_{re}$ , obtained using different methods when  $\gamma = 0.5$ . The black solid and red long-dashed lines represent the S1 and L1 trajectory results obtained by numerically solving the saddle point method, while the green dash-dot-dotted and brown short-dashed lines represent the S1 and L1 trajectory results obtained by the analytical method.

attributed to the nonadiabatic effect which increases HHG amplitude.

Based on the SFA theory, the velocity of the electron at the tunneling exit is determined by its motion under the barrier, and therefore, the nonadiabatic effect plays an important role in it. According to the analytical method, the tunneling exit velocity can be expressed as  $v_{ex} = p_s - A(t_{ex})$  and can also be expanded as

$$v_{ex} \approx p_s^{(5)} - A_{ex}^{(5)}, \quad (34)$$

where  $A_{ex}^{(5)}$  is the fifth-order expansion of  $A_{ex} \equiv A(t_{ex})$ . Generally, the complex tunneling exit velocity  $v_{ex}$  can also be obtained by numerical solution of saddle point equations, and its real part can be treated as the initial velocity of the electron to describe its classical dynamics later in the laser field.

In adiabatic theory, this velocity is always equal to zero, and it can be used as a criterion to judge whether a method is adiabatic or not [41]. Here the zero-order expansion of  $v_{ex}$  is equal to zero, which agrees with adiabatic approximation and is indicated as a gray dashed arrow line in Fig. 6(a). The real part of  $v_{ex}$  obtained by the numerical and nonadiabatic analytical methods are also plotted. It is obvious that the analytical results of the fifth-order expansion are far from  $v_{ex} = 0$  and vary with the kinetic energy of returned electron, aligning

with the nonadiabatic approximation in terms of velocity criteria [41]. Therefore, terms higher than zero truly describe the nonadiabatic effect.

The analytical result is in good agreement with the numerical one for the L1 trajectory. However, for the S1 trajectory, particularly in the low energy regions, the agreement is not as satisfactory. As previously mentioned, the perturbative analytical approach may not be well-suited for this particular case. This is because the effective adiabatic parameter  $\gamma(t_{ex})$  for the S1 trajectory is larger than  $\gamma$ , and even greater than 1. Fortunately, as illustrated in Fig. 5, when the entire ionization process is taken into account, the analytical HHG yield remains in good agreement with the numerical results.

In addition to velocity at the tunnel exit, the total energy at the tunnel exit also contains the nonadiabatic effect. It can be expressed as

$$E_{total} = v_{ex}^2/2 + E(t_{ex})r_{ex}. \quad (35)$$

Here,  $t_{ex}$  is still the tunneling exit time like we mentioned above. Therefore, the velocity  $v_{ex} = v(t_{ex})$  and displacement  $r_{ex} = r(t_{ex})$  at the tunneling exit can both be expanded using the analytical perturbation method. This expansion can also be applied to  $E_{total}$ . In adiabatic theory,  $\text{Re}[E_{total}]$  is always equal to  $-I_p$ , making it a useful criterion for determining if a method is adiabatic [41].

In Fig. 6 (b), comparisons between  $\text{Re}[E_{total}]$  obtained using different methods are displayed. The gray dashed arrow lines represent the result of the ADK adiabatic approximation where  $E_{total} = -I_p$ , providing a line of reference. When considering only the zero-order term, the same result  $E_{total} = -I_p$  can be directly obtained. Given that the vertical coordinates are in units of  $U_p$  and  $\gamma = 0.5$ , the gray dashed arrow lines are positioned at  $E_{total} = -0.5$ . It is evident that the green dash-dotted and black solid lines, representing the analytical FAE-S1 result and numerical NSFA-S1 result respectively, deviate significantly from the gray dashed arrow lines, particularly in the low energy region. Similarly, the brown short dashed and red dashed lines, obtained with the analytical and numerical methods for the L1 trajectory, also differ from the adiabatic result. Both the analytical and numerical methods are consistent with each other, especially for the L1 trajectory. Overall, the discrepancies mentioned above highlight the ability of the analytical method to uncover nonadiabatic effects.

## V. CONCLUSION

In this paper, we propose a fully analytical method that provides a detailed description of HHG. This method is based on SFA and combines the saddle point method with perturbation expansion. By expanding the ionization time, return time, and canonical momentum with respect to the Keldysh parameter, almost every physical quantity can be expressed as a function of the independent variable  $\tau_0$ , including the HHG yield. Therefore, approximate analytical solutions are provided without numerically solving the saddle point equations.

By comparing the HHG yields of different quantum trajectories obtained by the perturbative analytical method and the numerical saddle point method, we demonstrate that the perturbation analytical method is reliable for cases where  $\gamma \leq 0.27$  with a third-order expansion and  $\gamma \leq 0.65$  with a fifth-order expansion. Moreover, the accuracy of the analytical method is confirmed when considering the influence of the interference of different quantum trajectories. We demonstrate that TAE term of the HHG yield is a good approximation for the L1 trajectory, corresponding to a small effective adiabatic parameter, but is less accurate for the S1 trajectory, corresponding to a large effective adiabatic parameter. Including fifth-order expansion term results in good agreement with numerical results.

Furthermore, we propose a fifth-order scaling law. Our formulae show that the third-order scaling law relies on the binding energy and laser intensity only, while the fifth-order one relies on the laser wavelength in addition. Numerically, the fifth-order scaling law improves the accuracy of HHG yield by including the nonadiabatic effect. Physically, the third-order term of the HHG yield is only associated with the ionization process and resembles an ADK-like formula, which is in adiabatic approximation. However, the fifth-order term contains all the contributions from electron ionization, excursion and return processes.

Additionally, we find that the analytical method is equivalent to the ADK adiabatic approximation when only zero-order terms are considered. The fifth-order velocity and energy at the tunnel exit show that higher order expansion terms are nonadiabatic. The velocity at the tunnel exit is typically the initial velocity of the electron describing its classical dynamic motion out of the barrier in the laser field. Accounting for nonadiabatic effects in the initial velocity allows for a more accurate description of electron dynamics out of the barrier, leading to more precise HHG spectra.

## ACKNOWLEDGMENTS

This work was supported by the National Natural Science Foundation of China (Grant No. 12374322 and No. 12104501), the National Key Research and Development Program of China (Grant No. 2022YFE0111500), and NSF Investigator-Initiated Research (Grant No. 2208040). Thanks to Computing Center in Xi'an for the computing power support.

## Appendix A: The scaling process of saddle point equation

Based on Equation (12), Equation (8) can be rewritten in a more specific form as:

$$\frac{A_0^2}{2} \left[ \frac{\cos(t_r) - \cos(t_r - \tau)}{\tau} + \sin(t_r - \tau) \right]^2 = -I_p. \quad (A1)$$

When scaled by  $U_p$ , the equation above can be simplified to the form related to the adiabatic parameter  $\gamma$ :

$$\frac{1}{\tau}[\cos(t_r) - \cos(t_r - \tau)] + \sin(t_r - \tau) = \pm i\gamma. \quad (\text{A2})$$

The following will use the positive sign as an example. Here,  $t_r$  can be written as  $(t_r - \tau/2) + \tau/2$  and  $t_r - \tau$  can be written as  $(t_r - \tau/2) - \tau/2$ . Then, using trigonometric functions, one can obtain the following equation:

$$\begin{aligned} \sin(t_r - \tau/2)[\cos(\tau/2) - \frac{2\sin(\tau/2)}{\tau}] \\ - \cos(t_r - \tau/2)\sin(\tau/2) = i\gamma. \end{aligned} \quad (\text{A3})$$

Following the definitions  $a(\tau) = \cos(\tau/2) - 2\sin(\tau/2)/\tau$  and  $s(\tau) = \sin(\tau/2)$ , Eq. (A3) can be written in the form of Eq. (13).

### Appendix B: The derivation of the kinetic energy and return time of returned electron

As indicated in Eq. (8), the first term on the left side of the equation represents the electron velocity at the moment of ionization  $t_r$ , while the second term represents the electron velocity at the moment  $t_r - \tau$ . Referring to Eq. (12), one can determine the electron velocity at the return moment  $t_r$  as:

$$\begin{aligned} v(t_r) &= p_s - A(t_r) \\ &= A_0 \left[ \frac{\cos(t_r) - \cos(t_r - \tau)}{\tau} + \sin(t_r) \right]. \end{aligned} \quad (\text{B1})$$

By using the definition of  $a(\tau)$  and  $s(\tau)$ , the kinetic energy of the returned electron can be expressed as

$$E_{re} = 2U_p \left[ \sin\left(t_r - \frac{\tau}{2}\right) a(\tau) + \cos\left(t_r - \frac{\tau}{2}\right) s(\tau) \right]^2. \quad (\text{B2})$$

By utilizing the trigonometric identity  $\sin(t_r - \tau/2)^2 + \cos(t_r - \tau/2)^2 = 1$  in Eq. (13), we can derive the formula as

$$\sin\left(t_r - \frac{\tau}{2}\right) = \frac{i\gamma a(\tau) + s(\tau) \sqrt{a^2(\tau) + s^2(\tau) + \gamma^2}}{a^2(\tau) + s^2(\tau)}, \quad (\text{B3})$$

$$\cos\left(t_r - \frac{\tau}{2}\right) = \frac{-i\gamma s(\tau) + a(\tau) \sqrt{s^2(\tau) + a^2(\tau) + \gamma^2}}{s^2(\tau) + a^2(\tau)}. \quad (\text{B4})$$

By substituting Eqs. (B3) and Eq. (B4) into Eq. (B2), one can derive the kinetic energy of the returned electron as a function of  $\tau$ , expressed as Eq. (15). Therefore, it appears that the return time can be expressed as

$$t_r = \frac{\tau}{2} + \arctan \frac{\sin(t_r - \frac{\tau}{2})}{\cos(t_r - \frac{\tau}{2})}. \quad (\text{B5})$$

Inserting Eq. (B3) and Eq. (B4) into Eq. (B5) allows one to obtain the expression for the electron return time

$$\begin{aligned} t_r &= \frac{\tau}{2} + \\ &\arctan\left(\frac{a\sqrt{a^2 + \gamma^2 + s^2} - i s \gamma}{a^2 + s^2}, \frac{s\sqrt{a^2 + \gamma^2 + s^2} + i a \gamma}{a^2 + s^2}\right). \end{aligned} \quad (\text{B6})$$

### Appendix C: The derivation of the $\theta_5$

According to Equations (7) and (27),  $\theta$  is composed of two parts: the scaled quasiclassical action and the product of photon energy and return time. By scaling  $S(p_s, t_r, \tau) = (U_p/\omega)\alpha$  and  $\Omega t_r/\omega = (U_p/\omega)\beta$ ,  $\theta$  can be expressed as

$$\theta = \alpha + \beta. \quad (\text{C1})$$

Therefore, the FAE term of  $\theta$  can be expressed as

$$\theta_5 = \alpha_5 + \beta_5, \quad (\text{C2})$$

where  $\alpha_5$  and  $\beta_5$  are the fifth-order terms of  $\alpha$  and  $\beta$ , respectively. Starting from  $\beta$ , due to the relationship  $\Omega = E_{re} + I_p$ ,  $\beta$  can be expressed as

$$\beta = \frac{(E_{re} + I_p)}{U_p} t_r \quad (\text{C3})$$

Inserting Eqs.(20) and (22) to Eq.(C3), and keeping terms up to  $\gamma^5$ , one can obtain

$$\beta_5 = (E_{re2} + 2)t_{r3}. \quad (\text{C4})$$

As for  $\alpha$ , using the definition  $E(t) = E_0 \cos(t)$  then Eq. (12) can be used to replaced  $\mathbf{p}$  in Eq. (2). Then  $S(p_{st}, t_r, \tau)$  can be expressed as

$$S = \frac{1}{\omega} \int_{t_i}^{t_r} \left[ \frac{A_0^2 \left( \frac{\cos(t_r) - \cos(t_i)}{\tau} - \sin(t) \right)^2}{2} + I_p \right] dt. \quad (\text{C5})$$

Then scaling  $S(p_{st}, t_r, \tau)$  with  $(U_p/\omega)$ , one can obtain the expression of  $\alpha$  as

$$\alpha = 2 \int_{t_i}^{t_r} \left[ \left( \frac{\cos(t_r) - \cos(t_i)}{\tau} - \sin(t) \right)^2 + \gamma^2 \right] dt. \quad (\text{C6})$$

Solving integral Eq. (C6),  $\alpha$  can be rewritten as

$$\begin{aligned} \alpha &= 2\gamma^2\tau + \frac{-2 + 2\cos\tau + \tau^2}{\tau} + \\ &\frac{-\cos 2t_i + (2 - \tau \sin \tau) \cos(t_r + t_i) - \cos 2t_r}{\tau}. \end{aligned} \quad (\text{C7})$$

Based on the FAE method,  $\alpha_5$  can be expressed as a function as

$$\alpha_5 = \alpha_A + \alpha_B + \alpha_C + \alpha_D + \alpha_E + \alpha_F + \alpha_G. \quad (\text{C8})$$

Here  $\alpha_{A-G}$  are

$$\alpha_A = 2\tau_3 + 2\tau_1 t_{r2}^2 \cos 2(t_{i0}) + 2\tau_1^2 t_{r3} \cos(2t_{i0}) - \frac{2}{15} \tau_1^5 \cos(2t_{i0}) - 2\tau_1^2 \tau_3 \cos(2t_{i0}) + 2t_{r2} t_{r3} \sin(2t_{r0}) - 2t_{r2} t_{r3} \sin(2t_{i0}) \\ + \frac{4}{3} \tau_1^3 t_{r2} \sin(2t_{i0}) + 2\tau_3 t_{r2} \sin(2t_{i0}), \quad (C9)$$

$$\alpha_B = \frac{1}{\tau_0} \times \left[ -\frac{1}{60} \tau_1^5 \sin(\tau_0) - \tau_1^2 \tau_3 \sin(\tau_0) - \frac{4}{15} \tau_1^5 \sin(2t_{i0}) + \frac{1}{60} \tau_1^5 \sin(t_{r0} + t_{i0}) - 4\tau_1^2 \tau_3 \sin(2t_{i0}) + \tau_1^2 \tau_3 \sin(t_{r0} + t_{i0}) \right. \\ \left. + 4\tau_1 t_{r2}^2 \sin(2t_{i0}) - 4\tau_1 t_{r2}^2 \sin(t_{r0} + t_{i0}) + \frac{2}{3} \tau_1^3 t_{r2} \cos(t_{r0} + t_{i0}) + 4\tau_3 t_{r2} \cos(t_{r0} + t_{i0}) + 4t_{r2} t_{r3} \cos(2t_{r0}) \right. \\ \left. - 8t_{r2} t_{r3} \cos(t_{r0} + t_{i0}) + 4\tau_1^2 t_{r3} \sin(2t_{i0}) - 2\tau_1^2 t_{r3} \sin(t_{r0} + t_{i0}) \right] + \frac{4}{3} t_{r2} \cos(2t_{i0}) (-2\tau_1^3 - 3\tau_3 + 3t_{r3}), \quad (C10)$$

$$\alpha_C = -\frac{1}{12\tau_0^2} \times [24\tau_1 t_{r2}^2 \cos(2t_{r0}) - 8\tau_1(\tau_1^4 + 9\tau_1 \tau_3 - 6\tau_1 t_{r3} - 3t_{r2}^2) \cos(2t_{i0}) - 48\tau_1 t_{r2}^2 \cos(t_{r0} + t_{i0}) + \tau_1^5 \cos(t_{r0} + t_{i0}) \\ - 48\tau_1^2 t_{r3} \cos(t_{r0} + t_{i0}) + 36\tau_1^2 \tau_3 \cos(t_{r0} + t_{i0}) + \tau_1^5 \cos(\tau_0) + 36\tau_1^2 \tau_3 \cos(\tau_0) + 24\tau_3 t_{r2} \sin(2t_{r0}) \\ + 48\tau_1^3 t_{r2} \sin(2t_{i0}) + 24\tau_3 t_{r2} \sin(2t_{i0}) - 24(\tau_1^3 + 2\tau_3) t_{r2} \sin(t_{r0} + t_{i0})], \quad (C11)$$

$$\alpha_D = \frac{1}{3\tau_0^3} \times 2\tau_1^2 [(2\tau_1^3 + 9\tau_3) \sin(t_{r0} + t_{i0}) - (\tau_1^3 + 18\tau_3) \cos(t_{r0}) \sin(t_{r0} + t_{i0}) + 6\tau_1 t_{r2} \cos(2t_{i0}) - 6\tau_1 t_{r2} \cos(t_{r0} + t_{i0}) \\ + 12t_{r3} \sin^2\left(\frac{\tau_0}{2}\right) \sin(t_{r0} + t_{i0})], \quad (C12)$$

$$\alpha_E = -\frac{1}{3\tau_0^4} \times \tau_1^2 [6\tau_3 - 2(\tau_1^3 + 6\tau_3) \cos(t_{r0}) \cos(t_{i0}) + (2\tau_1^3 + 3\tau_3) \cos(t_{r0} + t_{i0}) + 8\tau_1 t_{r2} \sin^2\left(\frac{\tau_0}{2}\right) \sin(t_{r0} + t_{i0}) \\ + 3\tau_3 \cos(2t_{r0})], \quad (C13)$$

$$\alpha_F = -\frac{2\tau_1^5 [\sin(t_{r0} + t_{i0}) - 2 \cos(t_{r0}) \sin(t_{i0})]}{\tau_0^5}, \quad (C14)$$

$$\alpha_G = \frac{8\tau_1^5 [\sin^2\left(\frac{\tau_0}{2}\right) \sin^2\left(t_{r0} - \frac{\tau_0}{2}\right)]}{\tau_0^6}. \quad (C15)$$

By substituting Eq. (C4) and Eq. (C8) into Eq. (C2), one can obtain  $\theta_5$  in relation to ionization time, return time, and excursion time.

- 
- [1] A. McPherson, G. Gibson, H. Jara, U. Johann, T. S. Luk, I. A. McIntyre, K. Boyer, and C. K. Rhodes, Studies of multiphoton production of vacuum-ultraviolet radiation in the rare gases, *J. Opt. Soc. Am. B* **4**, 595 (1987).  
[2] M. Ferray, A. L'Huillier, X. F. Li, L. A. Lompre, G. Mainfray, and C. Manus, Multiple-harmonic conversion of 1064 nm radiation in rare gases, *J. Phys. B: At., Mol. Opt. Phys.* **21**, L31 (1988).  
[3] X. F. Li, A. L'Huillier, M. Ferray, L. A. Lompre, and G. Mainfray, Multiple-harmonic generation in rare gases at high laser intensity, *Phys. Rev. A* **39**, 5751 (1989).  
[4] S. Ghimire and D. A. Reis, High-harmonic generation from solids, *Nature Physics* **15**, 10 (2019).  
[5] N. Tancogne-Dejean and A. Rubio, Atomic-like high-harmonic generation from two-dimensional materials, *Sci. Adv.* **4**, eaao5207 (2018).  
[6] L. Yue and M. B. Gaarde, Characterizing anomalous high-harmonic generation in solids, *Phys. Rev. Lett.* **130**, 166903 (2023).  
[7] Y. Lang, Z. Peng, J. Liu, Z. Zhao, and S. Ghimire, Proposal for high-energy cutoff extension of optical harmonics of solid materials using the example of a one-dimensional ZnO crystal, *Phys. Rev. Lett.* **129**, 167402 (2022).  
[8] M. Guan, D. Chen, S. Hu, H. Zhao, P. You, and S. Meng, Theoretical insights into ultrafast dynamics in quantum materials, *Ultrafast Science* **2022**, 9767251 (2022).  
[9] T. T. Luu, Z. Yin, A. Jain, T. Gaumnitz, Y. Pertot, J. Ma, and H. J. Wörner, Extreme-ultraviolet high-harmonic generation in liquids, *Nature Communications* **9**, 3723 (2018).  
[10] A.-W. Zeng and X.-B. Bian, Impact of statistical fluctuations on high harmonic generation in liquids, *Phys. Rev. Lett.* **124**, 203901 (2020).

- [11] H. G. Kurz, D. S. Steingrube, D. Ristau, M. Lein, U. Morgner, and M. Kovačev, High-order-harmonic generation from dense water microdroplets, *Phys. Rev. A* **87**, 063811 (2013).
- [12] A. Mondal, O. Neufeld, Z. Yin, Z. Nourbakhsh, V. Svoboda, A. Rubio, N. Tancogne-Dejean, and H. J. Wörner, High-harmonic spectroscopy of low-energy electron-scattering dynamics in liquids, *Nature Physics* **19**, 1813 (2023).
- [13] G. Farkas and C. Tóth, Proposal for attosecond light pulse generation using laser induced multiple-harmonic conversion processes in rare gases, *Phys. Lett. A* **168**, 447 (1992).
- [14] P. M. Paul, E. S. Toma, P. Breger, G. Mullot, F. Augé, P. Balcou, H. G. Muller, and P. Agostini, Observation of a train of attosecond pulses from high harmonic generation, *Science* **292**, 1689 (2001).
- [15] M. Hentschel, R. Kienberger, C. Spielmann, G. A. Reider, N. Milosevic, T. Brabec, P. Corkum, U. Heinzmann, M. Drescher, and F. Krausz, Attosecond metrology, *Nature* **414**, 509 (2001).
- [16] J. Zhao and Z. Zhao, Probing  $\text{H}_2^+$  vibrational motions with high-order harmonic generation, *Phys. Rev. A* **78**, 053414 (2008).
- [17] Y. J. Chen, J. Liu, and B. Hu, Reading molecular messages from high-order harmonic spectra at different orientation angles, *J. Chem. Phys.* **130**, 044311 (2009).
- [18] C. Zhang, G. Brown, D. H. Ko, and P. B. Corkum, Optical measurement of photorecombination time delays, *Ultrafast Science* **3**, 0034 (2023).
- [19] D. Popmintchev, C. Hernández-García, F. Dollar, C. Mancuso, J. A. Pérez-Hernández, M.-C. Chen, A. Hankla, X. Gao, B. Shim, A. L. Gaeta, M. Tarazkar, D. A. Romanov, R. J. Levis, J. A. Gaffney, M. Foord, S. B. Libby, A. Jaron-Becker, A. Becker, L. Plaja, M. M. Murnane, H. C. Kapteyn, and T. Popmintchev, Ultraviolet surprise: Efficient soft x-ray high-harmonic generation in multiply ionized plasmas, *Science* **350**, 1225 (2015).
- [20] M. Lewenstein, P. Balcou, M. Y. Ivanov, A. L'Huillier, and P. B. Corkum, Theory of high-harmonic generation by low-frequency laser fields, *Phys. Rev. A* **49**, 2117 (1994).
- [21] R. Weissenbilder, S. Carlström, L. Rego, C. Guo, C. M. Heyl, P. Smorenburg, E. Constant, C. L. Arnold, and A. L'Huillier, How to optimize high-order harmonic generation in gases, *Nat. Rev. Phys.* **4**, 713 (2022).
- [22] K. Varjú, Y. Mairesse, B. Carré, M. B. Gaarde, P. Johnsson, S. Kazamias, R. López-Martens, J. Mauritsson, K. J. Schafer, P. Balcou, A. L'Huillier, and P. Salieres, Frequency chirp of harmonic and attosecond pulses, *J. Mod. Opt.* **52**, 379 (2005).
- [23] X. Xie, S. Yu, Y. Li, C. Zhang, Z. Yang, and Y. Chen, Odd-even harmonic emission from oriented no molecule with nodal planes, *Opt. Express* **33**, 14702 (2025).
- [24] L. Keldysh, Ionization in the field of a strong electromagnetic wave, *Sov. Phys. JETP* **20**, 1307 (1965).
- [25] F. J. Sun, C. Chen, W. Y. Li, X. Liu, W. Li, and Y. J. Chen, High ellipticity of harmonics from molecules in strong laser fields of small ellipticity, *Phys. Rev. A* **103**, 053108 (2021).
- [26] W. Becker, F. Grasbon, R. Kopold, D. Milošević, G. Paulus, and H. Walther, Above-threshold ionization: From classical features to quantum effects, *Adv. At. Mol. Opt. Phys.* **48**, 35 (2002).
- [27] I. A. Ivanov, A. S. Kheifets, A. Schimmoller, A. S. Landsman, and K. T. Kim, Evidence for nonzero electron velocity at the tunnel exit in strong-field atomic ionization, *Phys. Rev. Res.* **6**, 023049 (2024).
- [28] T. Moon, K. Bartschat, and N. Douguet, Strong-field ionization phenomena revealed by quantum trajectories, *Phys. Rev. Lett.* **133**, 073201 (2024).
- [29] A. M. Perelomov, V. S. Popov, and M. V. Terentev, Ionization of atoms in an alternating electric field, *Sov. Phys. JETP* **23**, 924 (1966).
- [30] M. V. Ammosov, N. B. Delone, and V. P. Krainov, Tunnel ionization of complex atoms and of atomic ions in an alternating electromagnetic field, *Sov. Phys. JETP* **64**, 1191 (1986).
- [31] N. B. Delone and V. P. Krainov, Energy and angular electron spectra for the tunnel ionization of atoms by strong low-frequency radiation, *J. Opt. Soc. Am. B* **8**, 1207 (1991).
- [32] S. Augst, D. Strickland, D. D. Meyerhofer, S. L. Chin, and J. H. Eberly, Tunneling ionization of noble gases in a high-intensity laser field, *Phys. Rev. Lett.* **63**, 2212 (1989).
- [33] L. Arissian, C. Smeenk, F. Turner, C. Trallero, A. V. Sokolov, D. M. Villeneuve, A. Staudte, and P. B. Corkum, Direct test of laser tunneling with electron momentum imaging, *Phys. Rev. Lett.* **105**, 133002 (2010).
- [34] N. Teeny, E. Yakaboylu, H. Bauke, and C. H. Keitel, Ionization time and exit momentum in strong-field tunnel ionization, *Phys. Rev. Lett.* **116**, 063003 (2016).
- [35] D. Trabert, N. Anders, S. Brennecke, M. S. Schöffler, T. Jahnke, L. P. H. Schmidt, M. Kunitski, M. Lein, R. Dörner, and S. Eckart, Nonadiabatic strong field ionization of atomic hydrogen, *Phys. Rev. Lett.* **127**, 273201 (2021).
- [36] Z. Wang, W. Quan, X. Hao, J. Chen, and X. Liu, The ellipticity dependence of rydberg state excitation of noble gas atoms subject to strong laser fields, *Front. Phys.* **11**, 1120654 (2023).
- [37] A. N. Pfeiffer, C. Cirelli, A. S. Landsman, M. Smolarski, D. Dimitrovski, L. B. Madsen, and U. Keller, Probing the longitudinal momentum spread of the electron wave packet at the tunnel exit, *Phys. Rev. Lett.* **109**, 083002 (2012).
- [38] P. Eckle, A. N. Pfeiffer, C. Cirelli, A. Staudte, R. Dörner, H. G. Muller, M. Büttiker, and U. Keller, Attosecond ionization and tunneling delay time measurements in helium, *Science* **322**, 1525 (2008).
- [39] R. Boge, C. Cirelli, A. S. Landsman, S. Heuser, A. Ludwig, J. Maurer, M. Weger, L. Gallmann, and U. Keller, Probing nonadiabatic effects in strong-field tunnel ionization, *Phys. Rev. Lett.* **111**, 103003 (2013).
- [40] M. Li, M.-M. Liu, J.-W. Geng, M. Han, X. Sun, Y. Shao, Y. Deng, C. Wu, L.-Y. Peng, Q. Gong, and Y. Liu, Experimental verification of the nonadiabatic effect in strong-field ionization with elliptical polarization, *Phys. Rev. A* **95**, 053425 (2017).
- [41] H. Ni, N. Eicke, C. Ruiz, J. Cai, F. Oppermann, N. I. Shvetsov-Shilovski, and L.-W. Pi, Tunneling criteria and a nonadiabatic term for strong-field ionization, *Phys. Rev. A* **98**, 013411 (2018).
- [42] N. Boroumand, A. Thorpe, A. M. Parks, and T. Brabec, Keldysh ionization theory of atoms: mathematical details, *J. Phys. B: At., Mol. Opt. Phys.* **55**, 213001 (2022).
- [43] Z. Xiao, W. Quan, S. Yu, X. Lai, X. Liu, Z. Wei, and J. Chen, Nonadiabatic strong field ionization of noble gas atoms in elliptically polarized laser pulses, *Opt. Express* **30**, 14873 (2022).
- [44] C. J. Lai, G. Cirmi, K. H. Hong, J. Moses, S. W. Huang, E. Granados, P. Keathley, S. Bhardwaj, and F. X. Kaertner, Wavelength scaling of high harmonic generation close to the multiphoton ionization regime, *Phys. Rev. Lett.* **111**, 073901 (2013).
- [45] D. R. Austin and J. Biegert, Strong-field approximation for the wavelength scaling of high-harmonic generation, *Phys. Rev. A* **86**, 023813 (2012).
- [46] G. Sansone, C. Vozzi, S. Stagira, and M. Nisoli, Nonadiabatic quantum path analysis of high-order harmonic generation: Role of the carrier-envelope phase on short and long paths, *Phys.*

- Rev. A **70**, 013411 (2004).
- [47] M. D. Spiewanowski, A. Etches, and L. B. Madsen, High-order harmonic generation from field-distorted orbitals, *Phys. Rev. A* **87**, 043424 (2013).
  - [48] R. Zuo, X. Song, S. Ben, T. Meier, and W. Yang, Revealing the nonadiabatic tunneling dynamics in solid-state high harmonic generation, *Phys. Rev. Research* **5**, L022040 (2023).
  - [49] A.-T. Le, H. Wei, C. Jin, and C. D. Lin, Strong-field approximation and its extension for high-order harmonic generation with mid-infrared lasers, *J. Phys. B: At., Mol. Opt. Phys.* **49**, 053001 (2016).
  - [50] X.-Z. Gao, A. S. Landsman, H. Cao, Y. Zhang, Y. Wang, Y. Fu, and L.-W. Pi, Influence of initial tunneling step on the return energy of high-order harmonic generation, *Phys. Rev. A* **106**, 053105 (2022).
  - [51] T. Augustine, F. Catoire, P. Agostini, L. F. DiMauro, C. C. Chirila, V. S. Yakovlev, and P. Salières, Driving-frequency scaling of high-harmonic quantum paths, *New J. Phys.* **14**, 103014 (2012).
  - [52] K. Midorikawa, Progress on table-top isolated attosecond light sources, *Nat. Photonics* **16**, 267 (2022).
  - [53] R. Schoenlein, T. Elsaesser, K. Holldack, Z. Huang, H. Kapteyn, M. Murnane, and M. Woerner, Recent advances in ultrafast x-ray sources, *Philosophical Transactions of the Royal Society A: Mathematical, Physical and Engineering Sciences* **377**, 20180384 (2019).
  - [54] S. P. Goreslavski, G. G. Paulus, S. V. Popruzhenko, and N. I. Shvetsov-Shilovski, Coulomb asymmetry in above-threshold ionization, *Phys. Rev. Lett.* **93**, 233002 (2004).
  - [55] M. V. Frolov, N. L. Manakov, A. A. Minina, S. V. Popruzhenko, and A. F. Starace, Adiabatic-limit coulomb factors for photoelectron and high-order-harmonic spectra, *Phys. Rev. A* **96**, 023406 (2017).